RadioGraphics

Informatics in Radiology (*info*RAD)

Introduction to the Language of Three-dimensional Imaging with Multidetector CT[1]

Neal C. Dalrymple, MD • Srinivasa R. Prasad, MD • Michael W. Freckleton, MD • Kedar N. Chintapalli, MD

The recent proliferation of multi–detector row computed tomography (CT) has led to an increase in the creation and interpretation of images in planes other than the traditional axial plane. Powerful three-dimensional (3D) applications improve the utility of detailed CT data but also create confusion among radiologists, technologists, and referring clinicians when trying to describe a particular method or type of image. Designing examination protocols that optimize data quality and radiation dose to the patient requires familiarity with the concepts of beam collimation and section collimation as they apply to multi–detector row CT. A basic understanding of the time-limited nature of projection data and the need for thin-section axial reconstruction for 3D applications is necessary to use the available data effectively in clinical practice. The axial reconstruction data can be used to create nonaxial two-dimensional images by means of multiplanar reformation. Multiplanar images can be thickened into slabs with projectional techniques such as average, maximum, and minimum intensity projection; ray sum; and volume rendering. By assigning a full spectrum of opacity values and applying color to the tissue classification system, volume rendering provides a robust and versatile data set for advanced imaging applications.
©RSNA, 2005

Introduction

The recent proliferation of multi–detector row computed tomography (CT) has led to an increase in the creation and interpretation of images in planes other than the axial images traditionally viewed with CT. Powerful three-dimensional (3D) applications improve the utility of detailed CT data but also create confusion among radiologists, technologists, and referring clinicians when trying to describe a particular method or type of image. Parallel advances that have been made in the areas of CT acquisition and image processing software are of comparable importance, since postprocessing cannot improve on the finite constraints of the acquired CT data and innovative imaging paradigms are needed to optimize the use of exquisite and voluminous data.

The following examples are proposed as a guide to terminology commonly used when acquiring and manipulating CT data to create multiplanar and 3D images. Specific topics discussed are collimation; projection data; data reconstruction; section thickness and interval; nominal and effective section thickness; the volumetric data set; multiplanar reformation; curved planar reformation; average, maximum, and minimum intensity projection; shaded surface display; volume rendering; and segmentation. Although the technical aspects of data acquisition discussed are specific to CT, many of the postprocessing principles apply to magnetic resonance (MR) imaging as well.

TAKE-HOME POINTS

- A basic understanding of the time-limited nature of projection data and the need for thin-section axial reconstruction for 3D applications is necessary for effective use of multi–detector row CT in clinical practice.

- Multiplanar images may be thickened into slabs by using projectional techniques such as average, maximum, and minimum intensity projection; ray sum; and volume rendering, depending on the anatomic structures of greatest interest.

- Volume rendering is a robust technique with diagnostic utility that far exceeds that of shaded surface display by combining a 3D perspective with versatile and interactive processing of the entire volume of reconstructed data.
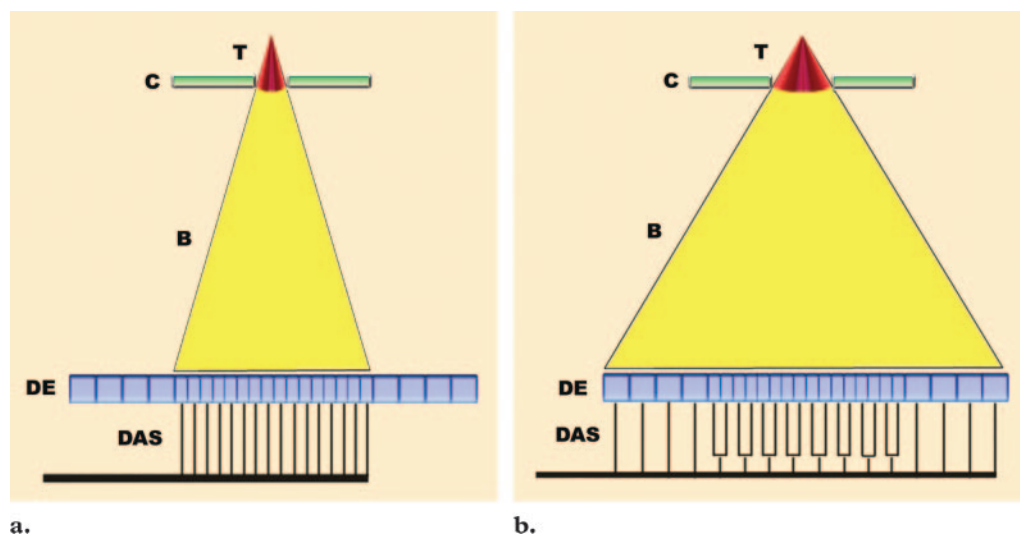
Collimation

The concept of collimation is relatively straightforward with single–detector row CT. With the single–detector row technique, collimation refers to the act of controlling beam size with a metallic aperture near the tube, thereby determining the amount of tissue exposed to the x-ray beam as the tube rotates around the patient (1,2). Thus, in single–detector row CT, there is a direct relationship between collimation and section thickness. Because the term *collimation* may be used in several different ways in multi–detector row CT, it is important to distinguish between beam collimation and section collimation.
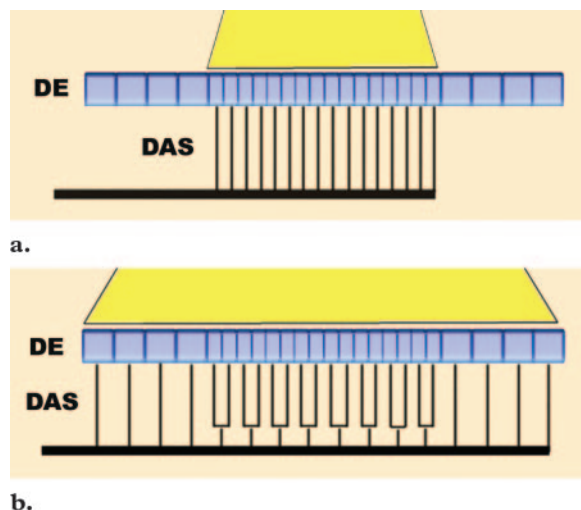
Beam Collimation

Beam collimation is the application of the same concept of collimation from single–detector row CT to multi–detector row CT. A collimator near the x-ray tube is adjusted to determine the size of the beam directed through the patient. Because multiple channels of data are acquired simultaneously, beam collimation is usually larger than reconstructed section thickness (3).

When a 16-channel scanner is used, for example, one of two settings is selected for most applications (Fig 1). Narrow collimation exposes only the central small detector elements. The data acquisition system controls the circuits that transmit data from the detector and collects data only from the intended elements (4,5). Wider collimation may expose the entire detector array. Unlike narrow collimation, in which the central elements are sampled individually, with wide collimation the 16 central elements are paired or binned, providing data as if they were eight larger elements (6). The four additional larger elements on each end of the detector array then complete the total of 16 channels of data. In this example, beam collimation would be 10 mm in the narrow setting or 20 mm in the wide setting.

Because beam collimation combined with table translocation determines the amount of z-axis coverage per rotation, it also helps determine the length of tissue or "volume coverage" that can be scanned within a given period (3). Larger beam collimation allows greater volume coverage within the time constraints of a given breath-hold or contrast material injection. An important point is that, as with single–detector row CT, narrow collimation in four- and 16-channel multi–detector row CT typically results in higher radiation dose to the patient compared with wide collimation (7,8).

RadioGraphics

a.   b.

Figure 1.   Beam collimation in 16-section CT. B = beam, C = collimator, DAS = data acquisition system, DE = detector elements, T = tube. **(a)** Narrow collimation exposes only the small central detector elements. **(b)** Wide collimation exposes all of the detector elements. The small central elements are paired or "binned" so that each pair acts as one larger element.

a.

b.

Figure 2.   Section collimation in multi–detector row CT. **(a)** Narrow collimation is coordinated with the data acquisition system *(DAS)* to allow use of the small central detector elements *(DE)* individually, resulting in 16 sections with a thickness of 0.6 mm each. This setting allows data reconstruction down to a section thickness of 0.6 mm. **(b)** Wide collimation is coordinated with the data acquisition system *(DAS)* to pair the 16 small central detector elements *(DE)* and use the eight peripheral elements individually, resulting in 16 sections with a thickness of 1.2 mm each. This setting allows data reconstruction down to a section thickness of 1.2 mm.

Section Collimation

The concept of section collimation is more complex but vital to understanding the potential of multi–detector row CT. One of the key components of multi–detector row CT is a detector array that allows partition of the incident x-ray beam into multiple subdivided channels of data (3). Section collimation defines the acquisition according to the small axial sections that can be reconstructed from the data as determined by how the individual detector elements are used to channel data. As opposed to beam collimation, which determines volume coverage, section collimation determines the minimal section thickness that can be reconstructed from a given data acquisition.

Using the earlier example of a 16-channel scanner, let us assume that the small central detector elements are 0.625 mm and the large peripheral elements are 1.25 mm. The size of the elements exposed and the way in which data are sampled from them by the data acquisition system determine the physical properties of the projection data used to generate axial images (4,6,8). When narrow collimation is applied (in this example, an incident beam width of 10 mm), the central small detector elements are treated individually by the data acquisition system (Fig 2). This form of acquisition permits reconstruction of axial sections as small as the central detector elements, or a section collimation of 0.625 mm.

When wide beam collimation (20 mm in this example) is used, the central elements are coupled so that two 0.625-mm elements are sampled as a single 1.25-mm element and the peripheral 1.25-mm elements are sampled individually, resulting in a section collimation of 1.25 mm. As a result, axial sections cannot be reconstructed smaller than 1.25 mm. Thus, section collimation is defined by the effective size of the channels of

Correlation between Beam Collimation and Section Collimation in Different Types of 16-Channel CT Scanners

Vendor of Scanner	Beam Collimation (mm)	Section Collimation (mm)
GE Healthcare*	20	1.25
	10	0.625
Philips,† Siemens‡	24	1.5
	12	0.75
Toshiba§	32	2.0
	16	1.0
	8	0.5

*GE Healthcare Technologies, Waukesha, Wis.
†Philips Medical Systems, Best, the Netherlands.
‡Siemens Medical Solutions, Erlangen, Germany.
§Toshiba Medical Systems, Tokyo, Japan.

Figure 3. Reconstruction of axial images from projection data. Projection data are never viewed directly. Rather, they are used to generate axial images. In multi–detector row CT, images used for primary axial interpretation usually have a section thickness several times larger than the minimum thickness available and may be called "thick sections." However, axial images can also be generated with a smaller section thickness, as determined by the section collimation. These are usually called "thin sections" and are essential for creating multiplanar reformatted and 3D images.

data sampled by the data acquisition system (the individual or coupled detector elements) and determines the minimum section thickness that can be reconstructed in a given acquisition mode. "Effective detector row thickness" is another term that has been used to describe section collimation (8).

If a routine abdominal examination interpreted at 5-mm section thickness reveals a finding and the radiologist or surgeon would like detailed coronal images, the section collimation determines whether the data can be reconstructed to 0.625-mm or 1.25-mm section thickness to provide a new data set for the reformatted images. Although it may be tempting to use the smallest section collimation available routinely, this may increase radiation dose to the patient (particularly with four- to 16-channel scanners) (7,8). Thus, section collimation is an important consideration in designing protocols with multi–detector row CT, as the anticipated need for isotropic data must be balanced with radiation dose considerations.

Section collimation and the quantity of data channels used during data acquisition are described by the term "detector configuration." For example, the detector configuration for a 16-channel scanner acquiring 16 channels of data, each 0.625 mm thick, is described as 16×0.625 mm. The same scanner could also acquire data by using different detector configurations, including 16×1.25 mm and 8×2.5 mm. The detector configuration also describes the relationship between section and beam collimation, since beam

collimation can be calculated as the product of the section collimation and the number of data channels used (5,8).

Although section profiles for thin and thick collimation vary among different vendors, the general principles are applicable to all scanners. Correlation between beam collimation and section collimation on different types of 16-channel scanners is shown in the Table.

Projection Data

Projection data are the initial product of CT acquisition prior to filtered back projection and the longitudinal interpolation necessary to create axial reconstructed sections. Projection data consist of line integrals and are never viewed directly but are used to generate axial images. There are several reasons to recognize projection data in clinical practice: *(a)* Spatial properties of the projection data are defined by scan acquisition and cannot be altered subsequently. *(b)* Only the projection data are used to reconstruct axial images, so any retrospective data reconstruction requires access to the projection data. *(c)* Projection data are not used directly to create 3D images. *(d)* In most cases, it is not practical to archive these large data sets, so access to generate volumetric data sets is time limited.

The finite constraints of the projection data make it necessary to anticipate which applications are likely to be helpful in the interpretation of a particular type of examination before it is performed so that data with the requisite z-axis or "through-plane" spatial resolution are available (1). When 3D reformations are likely to be beneficial, appropriate thin-section reconstructions must be performed before the projection data are
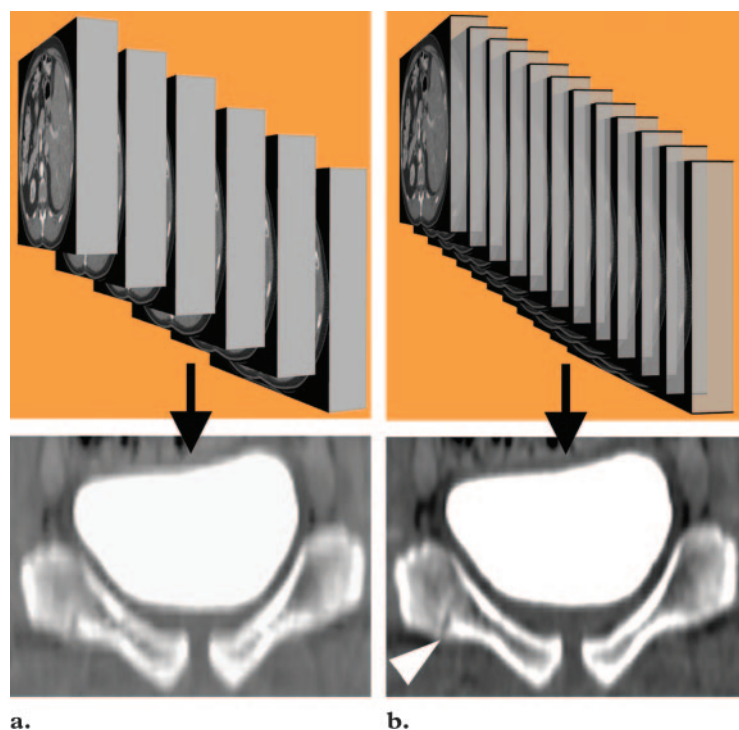
Figure 4. Effects of an overlapping reconstruction interval. **(a)** Contiguous data set reconstructed with a section thickness and interval of 2.5 mm. Coronal reformatted image shows a jagged cortical contour due to stair-step artifact. **(b)** Overlapping data set reconstructed with a section thickness of 2.5 mm but with the interval decreased to 1.25 mm, an overlap of 50%. Such overlapping minimizes stair-step artifact and improves demonstration of a fracture of the right superior pubic ramus (arrowhead).

deleted. With this in mind, routine secondary data reconstruction may be performed for certain categories of examinations. Increasing the data storage capacity of the scanner can prolong accessibility to the data, decreasing the chances of frustration that may occur when additional image reconstruction is desired after the projection data are no longer available.

Data Reconstruction

Data or image reconstruction refers to the process of generating axial images from projection data (Fig 3). Axial data sets can be viewed for interpretation or used to create multiplanar or 3D images. This requires increasingly sophisticated interpolation algorithms that take into account redundancies in overlapping data, effects of table speed, and geometric variability of the cone beam tube output (5,9,10). Section thickness, reconstruction interval, field of view, and convolutional kernel (reconstruction algorithm) must be specified each time data are reconstructed. Multiple data reconstructions can be performed automatically for a variety of reasons, such as including both soft-tissue and lung kernels of the chest or providing a thin-section data set for 3D applications. Additional retrospective data reconstruction can be performed as long as the projection data remain available (2).
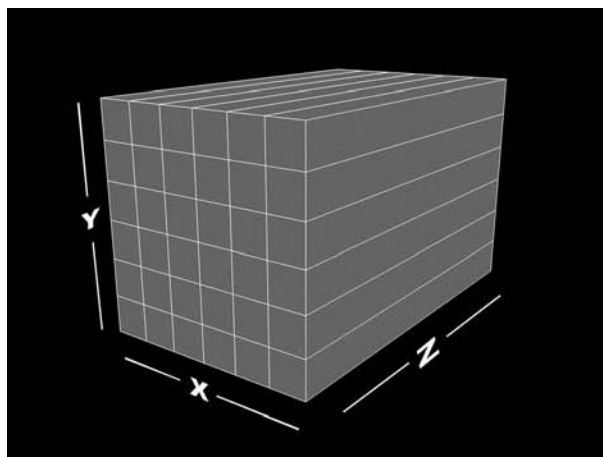
Section Thickness and Interval

Section thickness is the length of each segment of data along the z axis used during data reconstruc-

tion to calculate the value of each pixel on the axial images through a combination of helical interpolation and z-filtering algorithms (3,4,10–12). This determines the volume of tissue that will be included in the calculation to generate the Hounsfield unit value assigned to each of the pixels that make up the image (13). Reconstruction interval or increment refers to the distance along the z axis between the center of one transverse (axial) reconstruction and the next. Interval is independent of section thickness and can be selected arbitrarily since it is not limited by scan acquisition (2,14). When section thickness and interval are identical, images are considered to be contiguous.

In some cases, such as high-resolution CT of the chest, a small section thickness is selected to provide high spatial resolution but may be sampled at large intervals through the lung to obtain a representative sample with a limited number of images (eg, 1-mm section thickness at a 10-mm interval). Such discontinuous images are appropriate for evaluating generalized parenchymal disease in the lungs, but lung nodules can easily be missed. For 3D imaging, an overlapping interval is usually selected, meaning that the interval is smaller than the section thickness, usually by 50% (Fig 4) (14–17). For example, 1.25-mm sections can be reconstructed every 0.625 mm so that the

Figure 5.   Anisotropic and isotropic data. **(a)** Single–detector row CT performed with a nominal section thickness of 5 mm and a 512 × 512 matrix results in reconstructed data that are anisotropic, consisting of voxels with a facing pixel size of approximately 0.625 mm but a depth of 5 mm. This data set provides satisfactory axial images but has limited potential for secondary data reconstruction. **(b)** Sixteen-channel CT performed with wide collimation results in reconstructed data that are anisotropic, with a z-axis dimension (1.25 mm) approximately twice the size of the facing pixel (0.625 mm). By overlapping the reconstruction interval (which is not limited by section collimation), this data set provides excellent reformatted and volume-rendered images for many applications. **(c)** Sixteen-channel CT performed with narrow collimation results in reconstructed data that are isotropic, consisting of voxels that are relatively symmetric in all dimensions (0.625 mm). This data set provides exquisite data for multiplanar and 3D applications.

a.

b.

c.
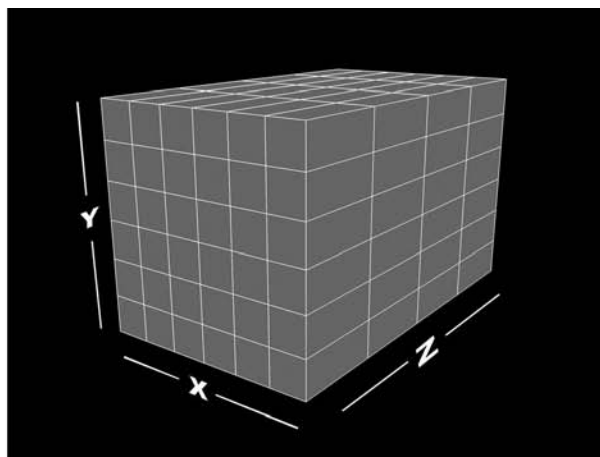
redundancy of data along the z axis results in smooth coronal or sagittal reformations. Although the section thickness is limited by the section collimation selected for scan acquisition, reconstruction interval is not limited by scan parameters (18). Even data reconstructed to the smallest section thickness available can be overlapped by using a smaller interval if necessary.

Nominal and Effective Section Thickness

As in single–detector row CT, table translation during scan acquisition and the interpolation algorithm used to generate axial sections have an effect on section thickness. Nominal section thickness is the section thickness specified by the collimation when a protocol is entered on the scanner. The actual section thickness of the reconstructed data is dependent not only on collimation but also on table speed and the method of z interpolation used (4,5,10,18–22). The term "effective section thickness" can be used to describe actual section thickness after broadening effects are taken into consideration (5). Some vendors provide this information on the image
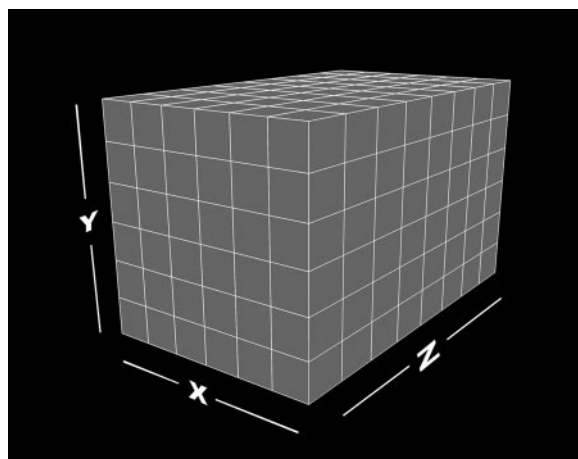
header or on the menu for image reconstruction (Philips Medical Systems, Siemens Medical Solutions, Toshiba Medical Systems); other vendors display only the nominal section thickness (GE Healthcare Technologies). Scan acquisition with a 16 × 1.25-mm detector configuration may result in effective section thickness of 1.3 mm with a low pitch and 1.5 mm with a higher pitch.

Volumetric Data Set

Although the diagnostic potential and sheer size of detailed CT data sets available with multi–detector row CT are likely to encourage integration
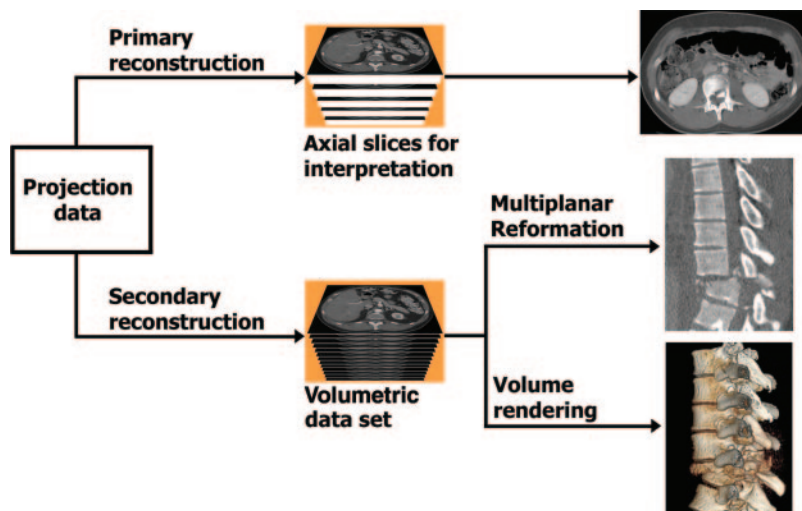
Figure 6.   Use of a volumetric data set. Projection data are typically used to reconstruct axial images of interpretive thickness for conventional review, which is performed by using printed film or with a picture archiving and communication system. Although it is occasionally useful to view thin axial images for osseous detail, axial viewing is usually performed with a section thickness of 3–5 mm. If necessary, a thin-section data set can be generated in addition to or in place of the traditional interpretive axial images. This may be called the volumetric data set because it is intended to be used not for primary axial interpretation but rather for generating high-quality multiplanar reformatted or volume-rendered images. This data set typically consists of axial images with a section thickness approaching 1 mm or even less, preferably with an overlapping interval.

of 3D imaging techniques into interpretation of even routine examinations (23), axial section interpretation remains an essential component of CT interpretation. While thin-section data sets may be reconstructed primarily when an examination is performed specifically for the purposes of CT angiography, colonography, or other advanced applications, 3D rendering techniques may also be useful for more routine examinations. To maintain acceptable contrast resolution on the primary axial interpretation sections, relatively thick sections are still reconstructed in most cases, typically ranging from 3 to 5 mm (8). Examinations performed with a field of view of 30–40 cm result in a pixel size of 0.5–0.8 mm on the axial sections, so a section thickness of 0.5–0.8 mm is required to generate a data set with similar spatial resolution in each dimension; such data are called isotropic data (Fig 5) (4,5,24,25).

Because only thin-section data with isotropic or near-isotropic properties provide diagnostic quality through-plane (long-axis) resolution, two

separate data sets are often reconstructed: *(a)* a primary reconstruction consisting of relatively thick sections for axial interpretation and *(b)* a volumetric data set consisting of thin overlapping sections for 3D rendering (Fig 6). Optimal results are usually achieved by selecting the smallest section thickness available from the raw projection data (26). As discussed earlier, only section thickness is limited by scan parameters, so sections can be reconstructed at an interval smaller than the section thickness, resulting in overlap of data along the z axis (eg, reconstruction of 1.25-mm-thick sections every 0.625 mm) (1,14,18,27).

Although projection data are stored on the scanner only for a limited time, a reconstructed thin-section data set can be archived on storage media or in a picture archiving and communication system, allowing access to high-quality image applications at a future date. Data reconstruction

Figure 7.   MPR. **(a)** Coronal reformatted image from routine abdominal-pelvic CT of a patient with bowel ischemia related to systemic lupus erythematosus vasculitis. Imaging in the coronal plane allowed visualization of bowel loop distribution throughout the abdomen and pelvis on a total of 28 images. Thickened distal loops of ileum are seen in the right lower quadrant with dilatation of more proximal small bowel loops. Arterial and venous patency was confirmed with this examination. **(b)** Sagittal reformatted image produced from CT data acquired with a trauma protocol. Examination of the chest, abdomen, and pelvis was performed with a detector configuration of 16×1.25 mm. Although a primary reconstruction thickness of 5 mm was used for axial interpretation, secondary data reconstruction to a section thickness of 1.25 mm at an interval of 0.625 mm allows a set of detailed full-spine sagittal images (approximately 20 1.5-mm-thick sections) to be created for every trauma case.

a.   b.

Figure 8.   Row of data encountered along a ray of projection. The data consist of attenuation information calculated in Hounsfield units. The value of the displayed two-dimensional pixel is determined by the amount of data included in the calculation (slab thickness) and the processing algorithm (maximum, minimum, or average intensity projection [AIP] or ray sum).
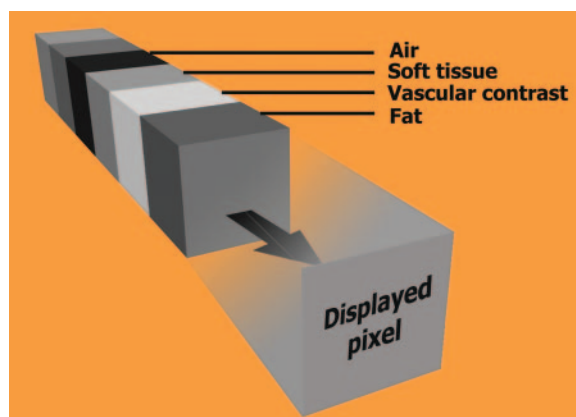
usually takes significantly longer than scan acquisition, and routine generation of large data sets can hinder scanner work flow at slow rates of reconstruction. If a scanner is purchased in anticipation of advanced 3D applications, rapid data reconstruction should be considered a priority.

Multiplanar Reformation

Multiplanar reformation (MPR) is the process of using the data from axial CT images to create nonaxial two-dimensional images (Fig 7). MPR images are coronal, sagittal, oblique, or curved plane images generated from a plane only 1 voxel in thickness transecting a set or "stack" of axial images (15,23,24,28). This technique is particularly useful for evaluating skeletal structures, since some fractures and joint alignment may not be readily apparent on axial sections.

Multiplanar images can be "thickened" into slabs by tracing a projected ray through the image to the viewer's eye, then processing the data encountered as that ray passes through the stack of reconstructed sections along the line of sight according to one of several algorithms (Fig 8) (24,29,30). Projectional techniques used in "thickening" of multiplanar images include maximum intensity projection (MIP), minimum intensity projection (MinIP), AIP, ray sum, and volume rendering and are sometimes called "multiplanar volume reformations" (31).

Curved Planar Reformation

Curved planar reformation is a type of MPR accomplished by aligning the long axis of the imaging plane with a specific anatomic structure, such as a blood vessel, rather than with an arbitrary imaging plane (15,16). Curved planar reforma-

a.   b.
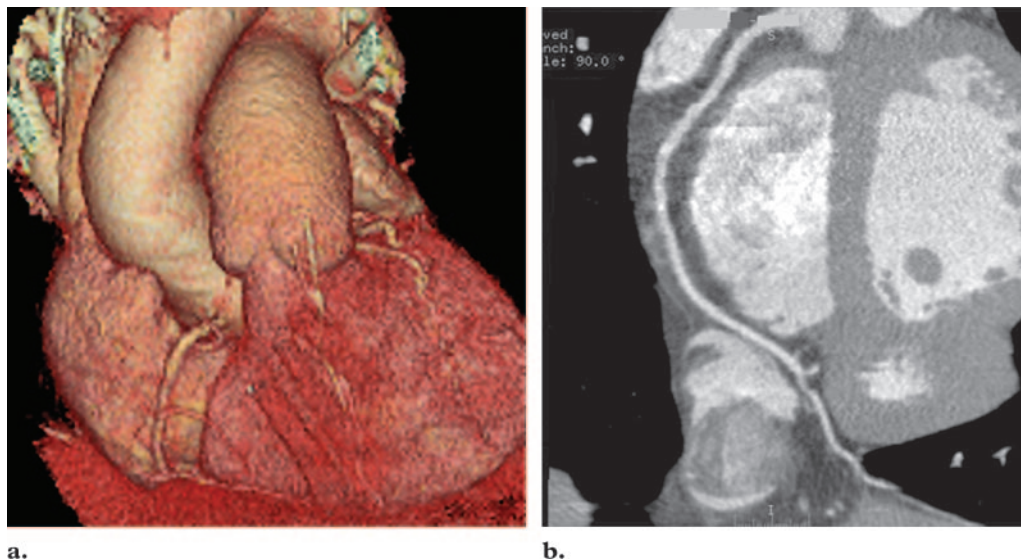
Figure 9.   Curved planar reformation. **(a)** Three-dimensional volume-rendered image shows the curved course of the right coronary artery. **(b)** Curved planar image of the right coronary artery shows a cross section of the vessel in its entirety. In this case, several points were selected along the course of the vessel on axial images; semiautomated software then defined an imaging plane that includes the entire length of the vessel. Because the imaging plane is defined by the vessel, other structures in the image are distorted.
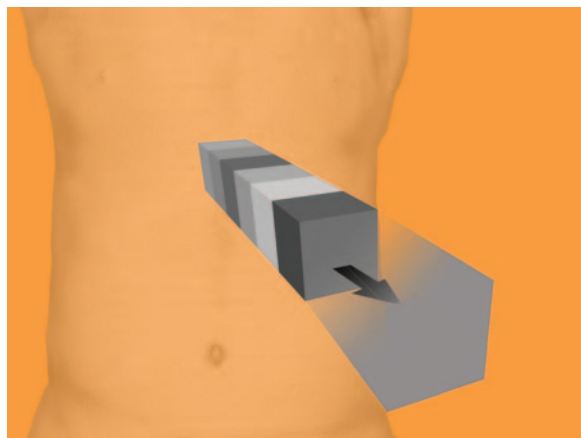
Figure 10.   AIP of data encountered by a ray traced through the object of interest to the viewer. The included data contain attenuation information ranging from that of air (black) to that of contrast media and bone (white). AIP uses the mean attenuation of the data to calculate the projected value.

tions can be created to include an entire structure on a single image. This is particularly useful in displaying an entire vessel, a ureter, or a long length of intestine, as these tubular structures are otherwise seen only by following them on consecutive images (Fig 9). Unlike surface- or volume-rendered 3D images, curved planar images display the cross-sectional profile of a vessel along its length, facilitating characterization of stenoses or other intraluminal abnormalities.

However, manual derivation of the curved plane can be time-consuming and may result in artifactual "pseudolesions." The recent introduc-

tion of automated methods for generating curved planar reformations has been shown to decrease user interaction time by 86% while maintaining image quality and actually decreasing the number of artifacts (32). The concept of thickening MPRs into slabs may be applied to curved planar reformations as well, resulting in curved slab reformations (33).

Average Intensity Projection
AIP describes one type of algorithm used to thicken MPRs. The image represents the average of each component attenuation value encountered by a ray cast through an object toward the viewer's eye (Fig 10). Starting with an MPR with a thickness of only 1 pixel (0.5–0.8 mm), thickening the multiplanar slab by using AIP may be

RadioGraphics

a.   b.

Figure 11. Effects of AIP on an image of the liver. **(a)** Coronal reformatted image created with a default thickness of 1 pixel (approximately 0.8 mm). **(b)** Increasing the slab thickness to 4 mm by using AIP results in a smoother image with less noise and improved contrast resolution. The image quality is similar to that used in axial evaluation of the abdomen.

used to produce images that have an appearance similar to traditional axial images with regard to low contrast resolution (Fig 11). This can be useful for characterizing the internal structures of a solid organ or the walls of hollow structures such as blood vessels or the intestine.

A different processing algorithm, ray sum, is offered on some workstations in place of or in addition to AIP. Rather than averaging the data along each projected ray tracing, ray sum simply adds all values, as the name implies (30). Therefore, full-volume ray sum images may have an appearance similar to that of a conventional radiograph. However, thin-slab ray sum produces images that appear similar to AIP images.

Maximum Intensity Projection

MIP images are achieved by displaying only the highest attenuation value from the data encountered by a ray cast through an object to the viewer's eye (Fig 12) (29,34). MIP is best used when the objects of interest are the brightest objects in the image (35) and is commonly used to evaluate contrast material–filled structures for CT angiography and CT urography. Large-volume MIP images have long been used to obtain 3D images from MR angiography data (30). Because only
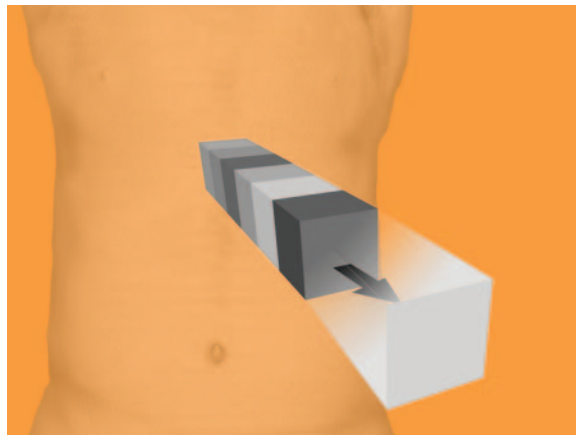
Figure 12. MIP of data encountered by a ray traced through the object of interest to the viewer. The included data contain attenuation information ranging from that of air (black) to that of contrast media and bone (white). MIP projects only the highest value encountered.

data with the highest value are used, MIP images usually contain 10% or less of the original data, a factor that was critical when computer processing power limited accessibility to advanced imaging techniques (35).

Thick-slab MIPs can also be applied to CT angiography data to include long segments of a vessel, but thin-slab MIP images (with section thickness less than 10 mm) viewed in sequence
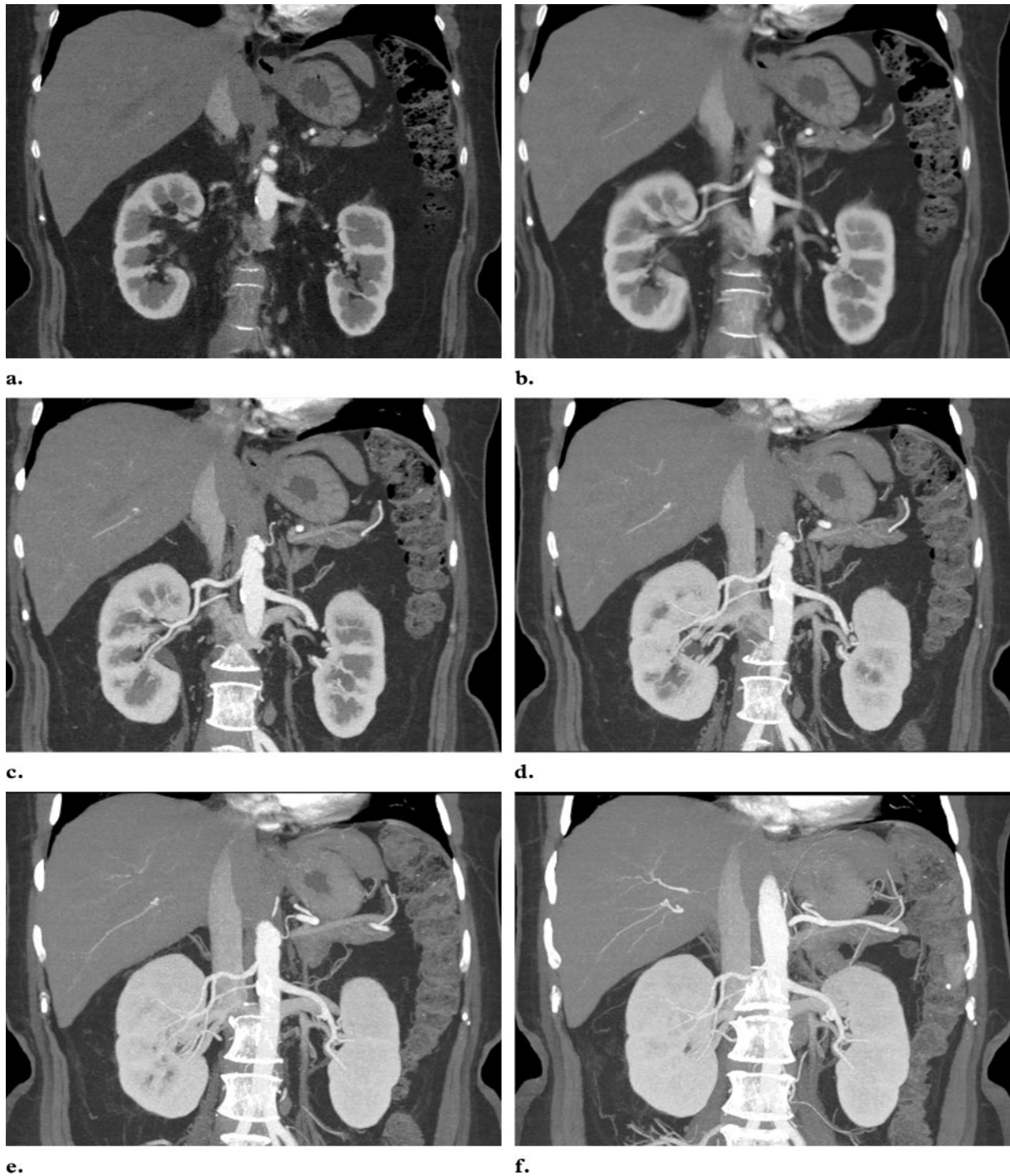
Figure 13.   Effects of MIP slab thickness on a coronal image of the abdomen. **(a, b)** Changing from the AIP technique **(a)** to the MIP technique **(b)** at a fixed slab thickness of 2.5 mm results in increased conspicuity of vessels. **(c–f)** More vessels are included per image as the section thickness increases to 5 mm **(c)**, 10 mm **(d)**, 15 mm **(e)**, and 20 mm **(f)**. However, use of thick slabs also results in obscuration of the vessels by other high-attenuation structures (bones, other vessels).

may provide more useful diagnostic information, as small structures are less likely to be obscured (Fig 13) (36,37). Although large-volume MIP images can demonstrate vessels in their entirety, the appreciation of 3D relationships between structures remains limited by a lack of visual cues that allow perception of depth relationships (16).

Figure 14.   MinIP of data encountered by a ray traced through the object of interest to the viewer. The included data contain attenuation information ranging from that of air (black) to that of contrast media and bone (white). MinIP projects only the lowest value encountered.

a.

b.
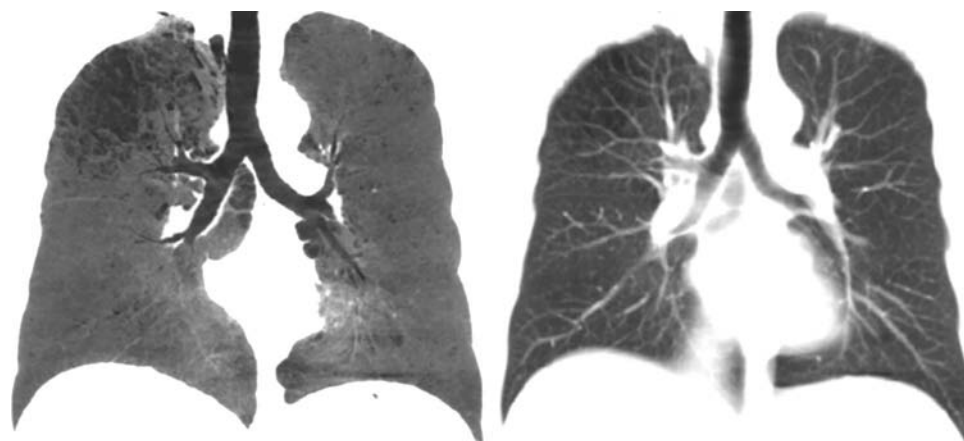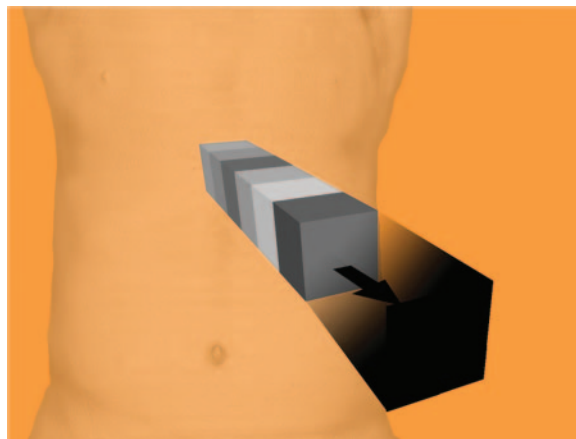
Figure 15.   Coronal slab image of the thorax (slab thickness = 20 mm) created with MinIP, AIP, and MIP. **(a)** On the MinIP image, the central airways are clearly demonstrated. Asymmetric emphysematous changes are seen in the right upper lobe. **(b)** On the AIP image, the central airways are not seen as well; the emphysematous changes remain visible but are less apparent. Interstitial and vascular structures within the lungs are seen better than on the MinIP image. **(c)** On the MIP image, the airways and emphysematous changes are obscured by vascular and soft-tissue structures. Longer segments of the vessels are visible than on the AIP image.

c.

RadioGraphics
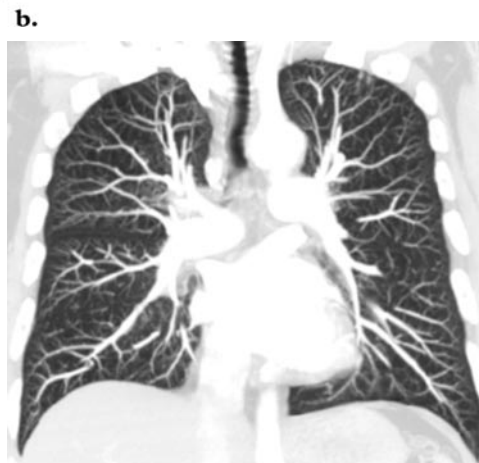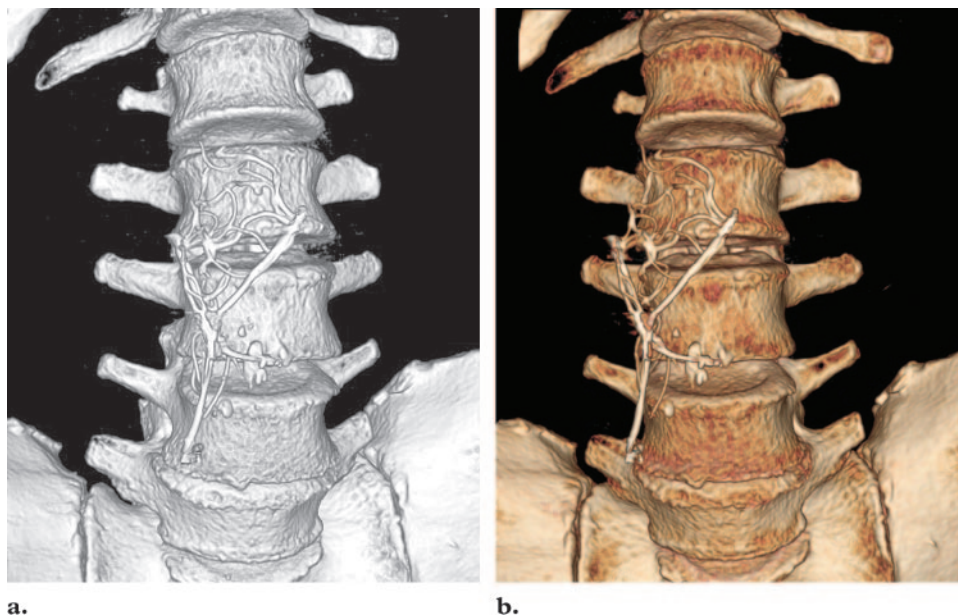
Figure 16. SSD and volume-rendered images of an inferior vena cava filter overlying the spine. **(a)** SSD creates an effective 3D model for looking at osseous structures in a more anatomic perspective than is achieved with axial images alone. It was used in this case to evaluate pelvic fractures not included on this image. **(b)** Volume rendering achieves a similar 3D appearance to allow inspection of the bone surfaces in a relatively natural anatomic perspective. In addition, the color assignment tissue classification possible with volume rendering allows improved differentiation of the inferior vena cava filter from the adjacent spine.

Minimum Intensity Projection

MinIP images are multiplanar slab images produced by displaying only the lowest attenuation value encountered along a ray cast through an object toward the viewer's eye (Fig 14). MinIP is not used commonly but may be used to generate images of the central airways or areas of air trapping within the lung (Fig 15) (38). These images may provide valuable perspective in defining lesions for surgical planning or detecting subtle small airway disease.

Shaded Surface Display

Shaded surface display (SSD), also called surface rendering, provides a 3D view of the surface of an object (Fig 16). The surface of an object must first be separated from other structures, a process called segmentation (discussed later). For osseous structures, this may be as simple as selecting a threshold that excludes soft-tissue structures. For other objects, segmentation may require meticulous editing. All data within the volume are in-

cluded in or excluded from the image on the basis of edge detection and/or thresholding, resulting in a binary data set (39–41).

A gray-scale shading procedure is then performed by using a formula to compute the observed light intensity in a given 3D scene, simulating surface reflections and shadowing from an artificial light source (40,42,43). The shading procedure assumes the presence of low-level ambient or diffuse light as well as a brighter, direct beam of light. Surfaces perpendicular to the beam of light have the highest levels of illumination whereas other surfaces appear shaded, similar to a surface relief map used to communicate surface terrain features in cartographic models (44). Combinations of direct and diffuse light result in a range of gray shades.

SSD has been used to demonstrate findings such as fractures after they are diagnosed on two-dimensional images (45). However, just as MIP

Figure 17. Data limitations of SSD. Surface data are segmented from other data by means of manual selection or an attenuation threshold. The graph in the lower part of the figure represents an attenuation threshold selected to include the brightly contrast-enhanced renal cortex and renal vessels during CT angiography. The "virtual spotlight" in the upper left corner represents the gray-scale shading process, which in reality is derived by means of a series of calculations. To illustrate the "hollow" data set that results from discarding all but the surface rendering data, the illustration was actually created by using a volume-rendered image of the kidney with a cut plane transecting the renal parenchyma. Subsequent editing was required to remove the internal features of the object while preserving the surface features of the original image. *HU* = Hounsfield units.
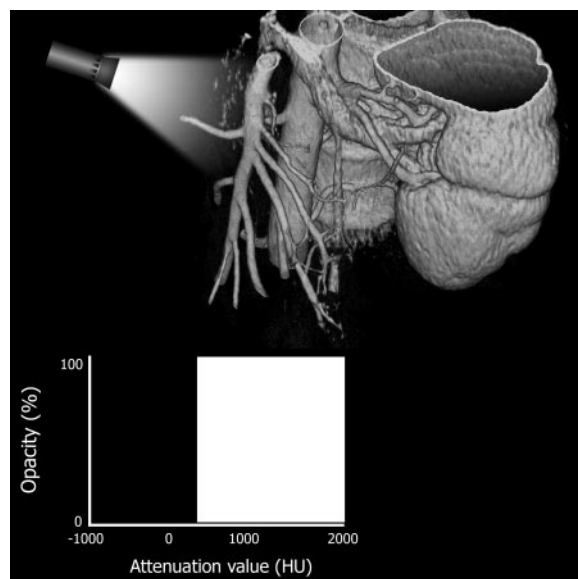
Figure 18. Data-rich nature of volume rendering. The graph in the lower part of the figure shows how attenuation data are used to assign values to a histogram-based tissue classification consisting of deformable regions for each type of tissue included. In this case, only fat, soft tissue, vessels, and bone are assigned values, but additional classifications can be added as needed. Opacity and color assignment may vary within a given region, and the shape of the region can be manipulated to achieve different image effects. Because there is often overlap in attenuation values between different tissues, the classification regions may overlap. Thus, accurate tissue and border classification may require additional mathematical calculations that take into consideration the characteristics of neighboring data. *HU* = Hounsfield units.
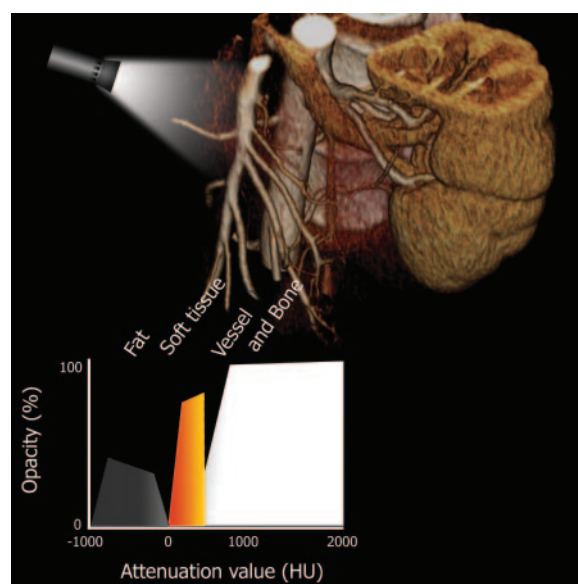
discards low-value data, SSD discards all but the surface-defining data, typically using less than 10% of the acquired data (Fig 17) (35,46). Although decreasing the amount of data was often an advantage when computer processing power was a limiting factor, this is no longer necessary and the binary nature of surface rendering limits flexibility of the data and makes it prone to undesirable artifacts (47). Volume rendering is now preferable to SSD for most if not all applications (38,45).

Volume Rendering

Volume rendering makes possible many of the advanced imaging applications performed on CT data at present. Using technology originally developed for motion picture computer animation (46,48), volume rendering assigns opacity values on a full spectrum from 0% to 100% (total transparency to total opacity) along an artificial line of sight projection using a variety of computational techniques (16,47). Because all acquired data may be used, volume rendering requires significantly greater processing power than MIP or surface rendering, limiting wide availability until relatively recent advances in computer hardware (17,39). Rectangular or trapezoidal classification schemes may be applied along the opacity spectrum, calculating the probability that a given voxel contains a specific tissue type (45), with separate classifications for tissues such as bone,

Figure 19. Three-dimensional volume-rendered image of a duplicated inferior vena cava. The color range selected is such that the opacity values of the partially contrast-enhanced venous structures are blue, whereas the more highly enhanced arterial structures are red. Color ramp was selected to achieve almost binary color assignment to avoid a graded appearance of the vessels.

soft tissue, contrast-enhanced vessels, air, and fat, depending on the clinical task at hand (48).

As in SSD, gray-scale shading is applied to simulate the surface reflections and shadowing of an artificial light source; however, more sophisticated calculations are possible using neighboring voxel values, since volumetric data are available (47–49). For example, instead of manual segmentation or an attenuation threshold being used to define a surface, abrupt changes in attenuation between adjacent voxels may signal a transition from one type of tissue to another. Some prefer the term "compositing" to describe the lighting effects performed in volume rendering (50). Although the 3D nature of volume rendering makes it appear similar to SSD, assigning a full spectrum of opacity values and separation of the tissue classification and shading processes provide a much more robust and versatile data set than the binary system offered by SSD (Fig 18) (47,51,52).

Volume rendering combines the use of opacity values and lighting effects to allow appreciation of spatial relationships between structures. However, there are limitations in perception if both tissue classification and surface shading are restricted to gray scale. By applying color to the histogram tissue classification system and reserving gray scale for the lighting effects, volume rendering uses the rapid data processing inherent in the human optical pathways to achieve intuitive perception of depth relationships in large data sets (16,53,54). Although the application of "pseudocolor" to tissue classification can be used to en-

hance discrimination between structures (Fig 19) (55–57), note that these color schemes do not represent the true optical color of the tissues.

In contrast to the predictable, linear progression of gray-scale values on conventional reconstructed axial CT images, the rate of progression in color assignment within tissue classifications and in regions of transition for volume rendering is tailored for particular applications. Although this is necessary to achieve the desired 3D effects, the arbitrary nature of color assignment must be acknowledged to avoid the mistakes that can occur by attributing significance to erroneous tissue classification (53). Such errors were more pronounced with attempts to apply color assignment to SSD and were often attributed to image noise, partial volume effects at tissue boundaries, user bias, and deviation of data from the assumed distribution in the applied histogram (58). However, similar pitfalls may be encountered with volume rendering as well.

One of the many strengths of volume rendering is the ability to select a variety of viewing perspectives. In addition to viewing angle and distance, schemes of perception may be applied to simulate specific types of visualization such as fiberoptic endoscopy. In general terms, volume rendering may be displayed as either orthographic or perspective volume rendering.

Orthographic Volume Rendering

Orthographic rendering is the most common method of display and assumes external visualization of an object, much like viewing a statue in a museum. Regardless of the viewing angle selected, display is based on the assumption that light rays reaching our eyes are parallel, similar to seeing objects from a great distance (24). As a result, structures are not distorted by proximity to the viewpoint (Fig 20).

Perspective Volume Rendering

Perspective volume rendering, sometimes called immersive rendering, assumes a viewpoint at a finite distance, usually from within a lumen, and is used to simulate fiberoptic endoscopy. Rather than light rays being parallel, projected light rays are focused to converge on the viewpoint, simulating natural light convergence on the human retina (24). The resulting distortion facilitates perception of distance on the basis of object size. Objects near the viewpoint appear large, whereas objects farther away appear small (25).

This technique can be applied to any type of lumen, although the most commonly described applications include evaluation of the colon, bronchial tree, urinary tract, and arteries (31,59–64). Perspective volume rendering can be helpful in planning endoscopic procedures and can facilitate an intuitive appreciation of relationships between anatomic structures (Fig 21). Whereas fiberoptic endoscopy is limited to visualization of the internal characteristics of a lumen, visual inspection with perspective volume rendering can be extended beyond the walls of the lumen to include adjacent extraluminal structures.

Segmentation

Segmentation is the process of selecting data to be included in a 3D image. Applying volume rendering or SSD to an entire scan volume often results in structures obscuring the object of interest. Segmentation allows some portions of the image to be selectively included or excluded using a variety of techniques. This process requires recognition of the tissue to be selected as well as delineation of precise spatial boundaries between tissues to be included and excluded (50).

Both tissue recognition and delineation can be performed automatically or with human assistance (65). Automated segmentation programs, which involve placement of a "seed" then expan-
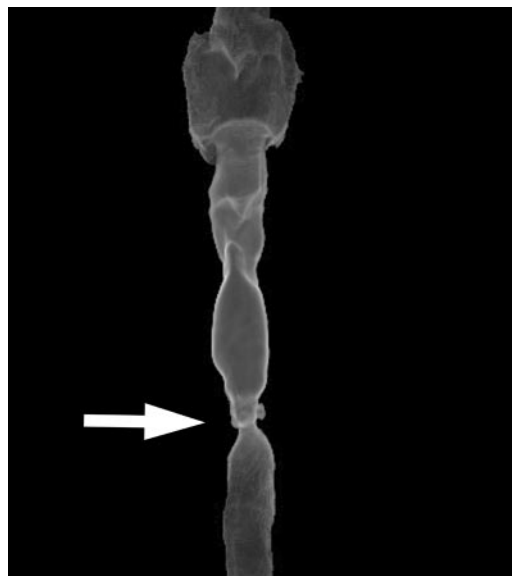

Figure 20.   Orthographic volume rendering of the airways. Volume-rendered image of a patient with tracheal stenosis (arrow) includes the airway from the hypopharynx to just above the carina. The image is not distorted by proximity or angle of the viewpoint and provides an "external" view of anatomic relationships. Segmentation of the airways was achieved by assigning a spike in opacity at the interface between air and soft-tissue attenuation. Overlying lung tissue was removed with region-of-interest editing to avoid obscuring the trachea.

sion of the region to be included or excluded using threshold-based algorithms, continue to improve and can rapidly remove the bones or isolate vascular structures. Because optimal segmentation may not be achieved with automated programs alone, several other basic forms of segmentation are available.

Region-of-Interest Editing

Region-of-interest editing is the most basic method of segmentation. A region of interest is removed by manually drawing a rectangular, elliptical, or other shape from within the data set using a sort of virtual scalpel to "cut" the defined region (Fig 22) (16). The delineated region is extruded through the volume along a linear path. Conversely, a region of interest can also be selected to be included in the image while all other data are excluded. Early programs required removal of objects on each axial image, while current software allows removal of objects from either two-dimensional or 3D images.

RadioGraphics
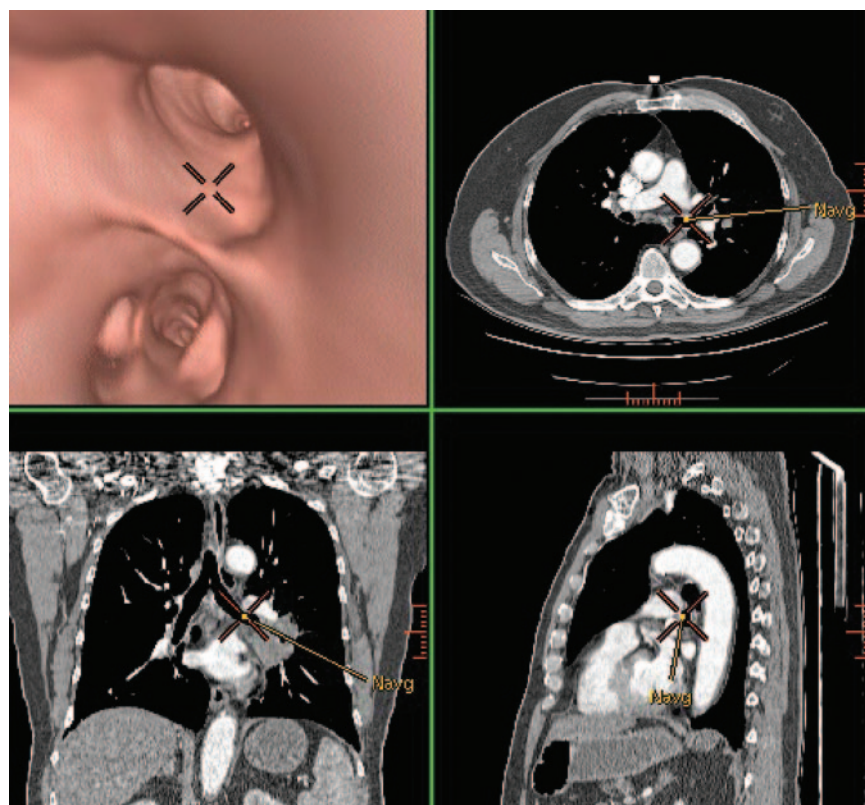
Figure 21. Perspective volume rendering of the airways. Axial (top right), coronal (bottom left), and sagittal (bottom right) chest CT scans show a left hilar mass, which is positioned between vascular structures. Virtual bronchoscopy (immersive rendering with a point of view within the tracheobronchial tree) (top left) was used to guide subsequent transbronchial biopsy, allowing six biopsy passes between central vascular structures without significant bleeding.


a.   b.   c.
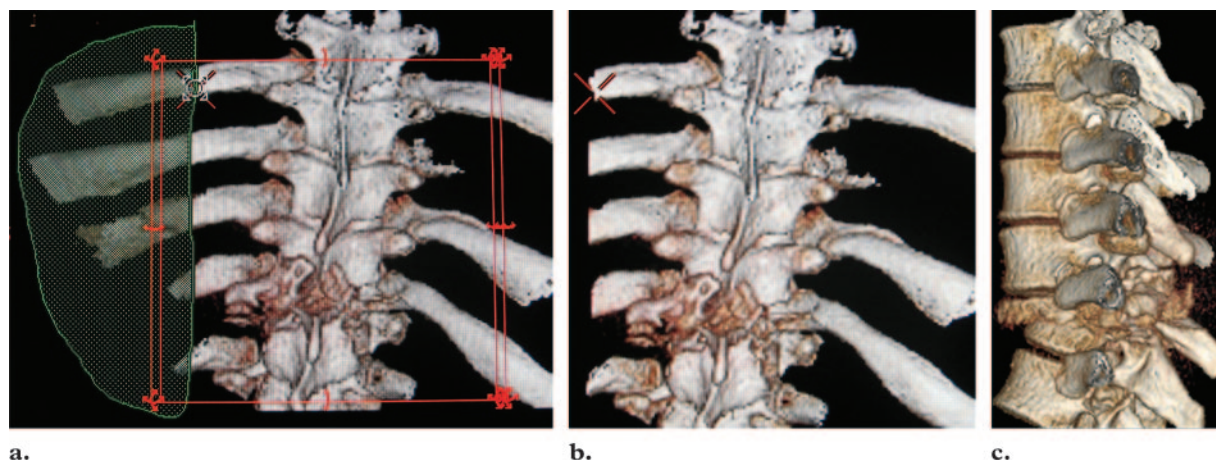
Figure 22. Region-of-interest editing. **(a)** Three-dimensional volume-rendered image (posterior view) from chest CT performed in a trauma patient with a fracture of T10. A region including a portion of the left ribs is defined manually (green area). **(b)** The selected region is then removed from the image. **(c)** Rib removal allows visualization of the fracture on a lateral projection without interference from overlying ribs.

Opacity Threshold

Because each data component of a volume-rendered image is assigned an opacity value, a threshold may be selected to determine the minimum opacity that is displayed. All data with values below the threshold are omitted from the image (Fig 23). Opacity thresholds have long been available

as a method of segmentation to facilitate removal of background structures in CT and MR angiography. This concept is particularly useful when applied to volume rendering of large tissue volumes. More soft-tissue structures can be added to
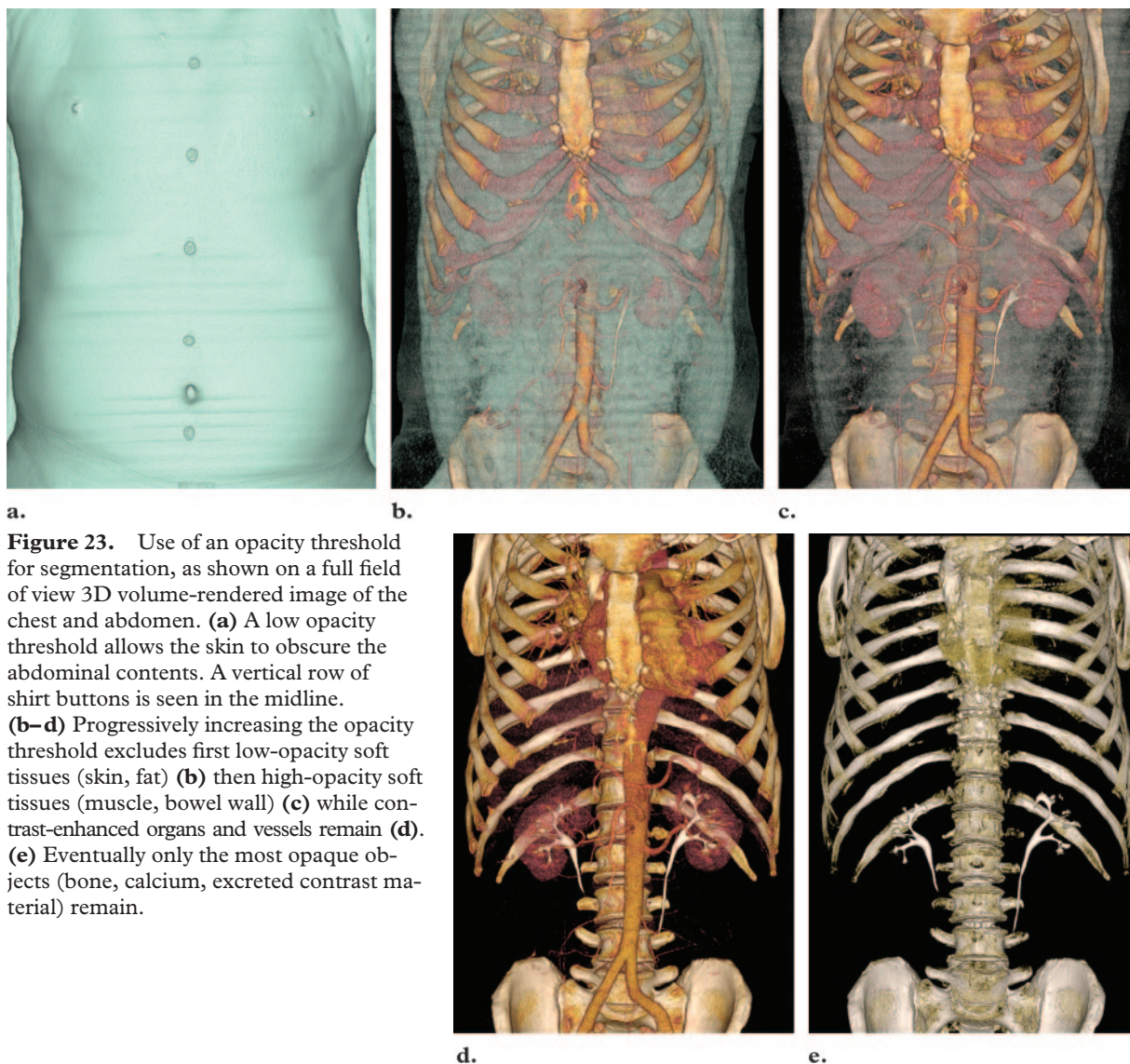
Figure 23. Use of an opacity threshold for segmentation, as shown on a full field of view 3D volume-rendered image of the chest and abdomen. **(a)** A low opacity threshold allows the skin to obscure the abdominal contents. A vertical row of shirt buttons is seen in the midline. **(b–d)** Progressively increasing the opacity threshold excludes first low-opacity soft tissues (skin, fat) **(b)** then high-opacity soft tissues (muscle, bowel wall) **(c)** while contrast-enhanced organs and vessels remain **(d)**. **(e)** Eventually only the most opaque objects (bone, calcium, excreted contrast material) remain.

the image by lowering the threshold. In addition to the threshold value, the curve that defines the rate of change in opacity assignment can be shaped to serve different purposes. Although linear curves are used most often, the curve can be adjusted to simulate a binary process such as SSD or to include only soft tissues while excluding air and bone.

Conclusions

The preceding examples are intended to clarify basic terminology used in some of the advanced 3D CT applications available today. Rapid progress in technology has not been matched by progress in physician and technologist education and training. Miscommunication and confusion may result in frustration and ineffective use of modern CT technology and postprocessing software. Designing examination protocols that optimize data quality and radiation dose to the patient requires familiarity with the concepts of beam and section collimation as they apply to multi–detector row CT. A basic understanding of the time-limited nature of projection data and the need for thin-section axial reconstruction for 3D applications is necessary to use the available data effectively in clinical practice.

We have reached a time, foreseen by some (23), when volumetric data can be archived for each CT examination, allowing exploration of the data with a variety of rendering techniques during initial interpretation or at a later date. Just as radiologists must understand the principles and pitfalls of ultrasonography to accurately interpret sonographic examinations and supervise sonographers, volumetric CT imaging requires an educated radiologist. Appreciation of the strengths

and weaknesses of available rendering techniques is essential to appropriate clinical application and is likely to become increasingly important as networked 3D capability can be used to integrate real-time rendering into routine image interpretation. Finally, educated technology users are better able to demand convenient and efficient forms of segmentation and image presentation, a demand that can be a driving force behind technology development.

References

1. Napel S. Basic principles of spiral CT. In: Fishman EK, Jeffrey RB Jr, eds. Spiral CT: principles, techniques, and clinical applications. Philadelphia, Pa: Lippincott-Raven, 1998; 3–15.

2. Hsieh J. A general approach to the reconstruction of x-ray helical computed tomography. Med Phys 1996;23:221–229.

3. Hu H. Multi-slice helical CT: scan and reconstruction. Med Phys 1999;26:5–18.

4. Prokop M, Galanski M. Spiral and multislice computed tomography of the body. New York, NY: Thieme, 2003.

5. Rydberg J, Liang Y, Teague SD. Fundamentals of multichannel CT. Radiol Clin North Am 2003;41: 465–474.

6. Cody DD, Davros W, Silverman PM. Principles of multislice computed tomographic technology. In: Silverman PM, ed. Multislice computed tomography: a practical approach to clinical protocols. Philadelphia, Pa: Lippincott Williams & Wilkins, 2002; 1–29.

7. McCollough CH, Zink FE. Performance evaluation of a multi-slice CT system. Med Phys 1999; 26:2223–2230.

8. Saini S. Multi–detector row CT: principles and practice for abdominal applications. Radiology 2004;233:323–327.

9. Flohr T, Stierstorfer K, Bruder H, Simon J, Schaller S. New technical developments in multislice CT. I. Approaching isotropic resolution with sub-millimeter 16-slice scanning. Rofo 2002;174: 839–845.

10. Hu H, He HD, Foley WD, Fox SH. Four multidetector-row helical CT: image quality and volume coverage speed. Radiology 2000;215:55–62.

11. Bruder H, Kachelriess M, Schaller S, Stierstorfer K, Flohr T. Single-slice rebinning reconstruction in spiral cone-beam computed tomography. IEEE Trans Med Imaging 2000;19:873–887.

12. Fuchs T, Krause J, Schaller S, Flohr T, Kalender WA. Spiral interpolation algorithms for multislice spiral CT. II. Measurement and evaluation of slice sensitivity profiles and noise at a clinical multislice system. IEEE Trans Med Imaging 2000;19:835–847.

13. Mahesh M. Search for isotropic resolution in CT from conventional through multiple-row detector. RadioGraphics 2002;22:949–962.

14. Kalender WA, Polacin A. Physical performance characteristics of spiral CT scanning. Med Phys 1991;18:910–915.

15. Rankin SC. Spiral CT: vascular applications. Eur J Radiol 1998;28:18–29.

16. Rubin GD. 3-D imaging with MDCT. Eur J Radiol 2003;45(suppl 1):S37–S41.

17. Rubin GD, Dake MD, Semba CP. Current status of three-dimensional spiral CT scanning for imaging the vasculature. Radiol Clin North Am 1995; 33:51–70.

18. Kalender WA, Polacin A, Suss C. A comparison of conventional and spiral CT: an experimental study on the detection of spherical lesions. J Comput Assist Tomogr 1994;18:167–176. [Published correction appears in J Comput Assist Tomogr 1994;18(4):671.]

19. Brink JA, Heiken JP, Balfe DM, Sagel SS, DiCroce J, Vannier MW. Spiral CT: decreased spatial resolution in vivo due to broadening of section-sensitivity profile. Radiology 1992;185:469–474.

20. Kalra MK, Maher MM, Toth TL, et al. Strategies for CT radiation dose optimization. Radiology 2004;230:619–628.

21. Polacin A, Kalender WA, Marchal G. Evaluation of section sensitivity profiles and image noise in spiral CT. Radiology 1992;185:29–35.

22. Wang GM, Redford K, Zhao S, Vannier MW. A study on the section sensitivity profile in multirow-detector CT. J X-Ray Sci Tech 2003;11:1–11.

23. Rubin GD, Napel S, Leung AN. Volumetric analysis of volumetric data: achieving a paradigm shift [editorial]. Radiology 1996;200:312–317.

24. Rubin GD. Multislice imaging for three-dimensional examinations. In: Silverman PM, ed. Multislice helical tomography: a practical approach to clinical protocols. Philadelphia, Pa: Lippincott Williams & Wilkins, 2002; 317–324.

25. Rubin GD, Beaulieu CF, Argiro V, et al. Perspective volume rendering of CT and MR images: applications for endoscopic imaging. Radiology 1996;199:321–330.

26. Kim DO, Kim HJ, Jung H, Jeong HK, Hong SI, Kim KD. Quantitative evaluation of acquisition parameters in three-dimensional imaging with multidetector computed tomography using human skull phantom. J Digit Imaging 2002;15(suppl 1): 254–257.

27. Ney DR, Fishman EK, Magid D, Robertson DD, Kawashima A. Three-dimensional volumetric display of CT data: effect of scan parameters upon image quality. J Comput Assist Tomogr 1991;15: 875–885.

28. Rubin GD, Silverman SG. Helical (spiral) CT of the retroperitoneum. Radiol Clin North Am 1995; 33:903–932.

29. Calhoun PS, Kuszyk BS, Heath DG, Carley JC, Fishman EK. Three-dimensional volume rendering of spiral CT data: theory and method. RadioGraphics 1999;19:745–764.

30. Keller PJ, Drayer BP, Fram EK, Williams KD, Dumoulin CL, Souza SP. MR angiography with two-dimensional acquisition and three-dimensional display: work in progress. Radiology 1989; 173:527–532.

31. Boiselle PM. Multislice helical CT of the central airways. Radiol Clin North Am 2003;41:561–574.

32. Raman R, Napel S, Beaulieu CF, Bain ES, Jeffrey RB Jr, Rubin GD. Automated generation of curved planar reformations from volume data:

method and evaluation. Radiology 2002;223:275–280.

33. Raman R, Napel S, Rubin GD. Curved-slab maximum intensity projection: method and evaluation. Radiology 2003;229:255–260.

34. Napel S, Marks MP, Rubin GD, et al. CT angiography with spiral CT and maximum intensity projection. Radiology 1992;185:607–610.

35. Heath DG, Soyer PA, Kuszyk BS, et al. Three-dimensional spiral CT during arterial portography: comparison of three rendering techniques. RadioGraphics 1995;15:1001–1011.

36. Kim JK, Kim JH, Bae SJ, Cho KS. CT angiography for evaluation of living renal donors: comparison of four reconstruction methods. AJR Am J Roentgenol 2004;183:471–477.

37. Napel S, Rubin GD, Jeffrey RB Jr. STS-MIP: a new reconstruction technique for CT of the chest. J Comput Assist Tomogr 1993;17:832–838.

38. Ravenel JG, McAdams HP. Multiplanar and three-dimensional imaging of the thorax. Radiol Clin North Am 2003;41:475–489.

39. Fishman EK, Magid D, Ney DR, et al. Three-dimensional imaging. Radiology 1991;181:321–337. [Published correction appears in Radiology 1992;182(3):899.]

40. Magnusson M, Lenz R, Danielsson PE. Evaluation of methods for shaded surface display of CT volumes. Comput Med Imaging Graph 1991;15:247–256.

41. van Ooijen PM, van Geuns RJ, Rensing BJ, Bongaerts AH, de Feyter PJ, Oudkerk M. Noninvasive coronary imaging using electron beam CT: surface rendering versus volume rendering. AJR Am J Roentgenol 2003;180:223–226.

42. Rubin GD, Dake MD, Napel S, et al. Spiral CT of renal artery stenosis: comparison of three-dimensional rendering techniques. Radiology 1994;190:181–189.

43. Rubin GD, Dake MD, Napel SA, McDonnell CH, Jeffrey RB Jr. Three-dimensional spiral CT angiography of the abdomen: initial clinical experience. Radiology 1993;186:147–152.

44. Bolstad P. Terrain analysis. In: GIS fundamentals: a first text on geographic information systems. White Bear Lake, Minn: Eider, 2002; 297–298.

45. Kuszyk BS, Heath DG, Bliss DF, Fishman EK. Skeletal 3-D CT: advantages of volume rendering over surface rendering. Skeletal Radiol 1996;25:207–214.

46. Fishman EK, Drebin B, Magid D, et al. Volumetric rendering techniques: applications for three-dimensional imaging of the hip. Radiology 1987;163:737–738.

47. Levoy M. Display of surfaces from volume data. IEEE Comput Graph Appl 1988;8:29–37.

48. Drebin RA, Hanrahan P. Volume rendering. Comput Graph 1988;22:65–74.

49. Hohne KH. Shading 3D-images from CT using gray level gradients. IEEE Trans Med Imaging 1986;1:45–47.

50. Udupa JK. Three-dimensional visualization and analysis methodologies: a current perspective. RadioGraphics 1999;19:783–806.

51. Fishman EK, Drebin RA, Hruban RH, Ney DR, Magid D. Three-dimensional reconstruction of the human body. AJR Am J Roentgenol 1988;150:1419–1420.

52. Fishman EK, Magid D, Ney DR, Drebin RA, Kuhlman JE. Three-dimensional imaging and display of musculoskeletal anatomy. J Comput Assist Tomogr 1988;12:465–467.

53. Vannier MW, Rickman D. Multispectral and color-aided displays. Invest Radiol 1989;24:88–91.

54. Ward J, Magnotta V, Andreasen NC, Ooteman W, Nopoulos P, Pierson R. Color enhancement of multispectral MR images: improving the visualization of subcortical structures. J Comput Assist Tomogr 2001;25:942–949.

55. Brown HK, Hazelton TR, Fiorica JV, Parsons AK, Clarke LP, Silbiger ML. Composite and classified color display in MR imaging of the female pelvis. Magn Reson Imaging 1992;10:143–154. [Published correction appears in Magn Reson Imaging 1992;10(3):495.]

56. Brown HK, Hazelton TR, Parsons AK, Fiorica JV, Berman CG, Silbiger ML. PC-based multiparameter full-color display for tissue segmentation in MRI of adnexal masses. J Comput Assist Tomogr 1993;17:993–1005.

57. Brown HK, Hazelton TR, Silbiger ML. Generation of color composites for enhanced tissue differentiation in magnetic resonance imaging of the brain. Am J Anat 1991;192:23–34.

58. Cline HE, Lorensen WE, Kikinis R, Jolesz F. Three-dimensional segmentation of MR images of the head using probability and connectivity. J Comput Assist Tomogr 1990;14:1037–1045.

59. Hara AK, Johnson CD, Reed JE, Ehman RL, Ilstrup DM. Colorectal polyp detection with CT colography: two- versus three-dimensional techniques—work in progress. Radiology 1996;200:49–54.

60. Kimura F, Shen Y, Date S, Azemoto S, Mochizuki T. Thoracic aortic aneurysm and aortic dissection: new endoscopic mode for three-dimensional CT display of aorta. Radiology 1996;198:573–578.

61. McAdams HP, Goodman PC, Kussin P. Virtual bronchoscopy for directing transbronchial needle aspiration of hilar and mediastinal lymph nodes: a pilot study. AJR Am J Roentgenol 1998;170:1361–1364.

62. Sommer FG, Olcott EW, Ch'en I, Beaulieu CF. Volume rendering of CT data: applications to the genitourinary tract. AJR Am J Roentgenol 1997;168:1223–1226. [Published correction appears in AJR Am J Roentgenol 1997;169(2):602.]

63. Vining DJ, Zagoria RJ, Liu K, Stelts D. CT cystoscopy: an innovation in bladder imaging. AJR Am J Roentgenol 1996;166:409–410.

64. Smith PA, Heath DG, Fishman EK. Virtual angioscopy using spiral CT and real-time interactive volume-rendering techniques. J Comput Assist Tomogr 1998;22:212–214.

65. Fishman EK, Liang CC, Kuszyk BS, et al. Automated bone editing algorithm for CT angiography: preliminary results. AJR Am J Roentgenol 1996;166:669–672.